Estimating individual level plant traits at scale

Sergio Marconi[1]*, Sarah J. Graves[2,3], Ben. G. Weinstein[4], Stephanie Bohlman[2], Ethan P. White[4]

[1]School of Natural Resources and Environment, University of Florida, Gainesville, FL, 32611 USA

[2]School of Forest Resources and Conservation, University of Florida, Gainesville, FL 32603, USA

[3]University of Wisconsin-Madison, Nelson Institute for Environmental Studies, Madison, WI, United States, 53706

[4]Department of Wildlife Ecology and Conservation, University of Florida, Gainesville, FL 32603, USA

Corresponding author: Sergio Marconi, sergio.marconi@weecology.org

Abstract

Functional ecology has increasingly focused on describing ecological communities based on their traits (measurable features affecting individuals fitness and performance). Analyzing trait distributions within and among forests could significantly improve understanding of community composition and ecosystem function. Historically, data on trait distributions are generated by (1) collecting a small number of leaves from a small number of trees, which suffers from limited sampling but produces information at the fundamental ecological unit (the individual); or (2) using remote sensing images to infer traits, producing information continuously across large regions, but as plots (containing multiple trees of different species) or pixels, not individuals. Remote sensing methods that identify individual trees and estimate their traits would provide the benefits of both approaches, producing continuous large-scale data linked to biological individuals. We used data from the National Ecological Observatory Network (NEON) to develop a method to scale up functional traits from 160 trees to the millions of trees within the spatial extent of two NEON sites. The pipeline consists of three stages: 1) image segmentation, to identify individual trees and estimate structural traits; 2) ensemble of models to infer leaf mass area (LMA), nitrogen, carbon, and phosphorus content using hyperspectral signatures, and DBH from allometry; and 3) predictions for segmented crowns for the full remote sensing footprint at the NEON sites.

The R^2 values on held out test data ranged from 0.41 to 0.75 on held out test data. The ensemble approach performed better than single partial least squares models. Carbon performed poorly compared to other traits (R^2 of 0.41). The crown segmentation step contributed the most uncertainty in the pipeline, due to over-segmentation. The pipeline produced good estimates of DBH (R^2 of 0.62 on held out data). Trait predictions for crowns performed significantly better

than comparable predictions on pixels, resulting in improvement of R^2 on test data of between 0.07 to 0.26. We used the pipeline to produce individual level trait data for ~5 million individual crowns, covering a total extent of ~360 km^2. This large dataset allows testing ecological questions on landscape scales, revealing that foliar traits are correlated with structural traits and environmental conditions.

Keywords: Plant traits, Foliar, Structural, NEON, Hyperspectral, LiDAR, Individual Tree Crown

1. Introduction

Functional traits are biochemical, physiological and structural characters that influence organism performance or fitness (Nock et al., 2016). They are central to how organisms perform under different environmental conditions, interact with other species, and influence the ecosystems to which they belong (McGill 2006, Dwyer et al., 2017, Collalti et al., 2019). For individual organisms, traits influence core demographic parameters including survival and reproduction. At the species level, traits influence species distributions and how species respond to changes in land use and climate (Pollock et al., 2012). At the ecosystem level, organismal traits influence biogeochemical cycles and habitat availability for other species (e.g., Fisichelli et al., 2015). Given their central importance across multiple levels of organization, understanding how traits vary within and among species, across environmental gradients, and through time is essential to understanding many areas of ecology and predicting how ecological systems will change in the future (McGill 2006, Lawler et al. 2010, Valladares et al., 2014, Diaz et al., 2016).

In trees, two commonly studied groups of traits are specific to (1) properties of leaves (e.g. , leaf mass per area, nitrogen and phosphorus concentration) and (2) the size structure of the full tree (e.g. height, dbh, canopy size). These characters hold different information about tree properties and how they link to forest functions. Nitrogen and phosphorus, for example, are fundamental proxies of leaf productivity because of their fundamental role in photosynthesis (Tang et al., 2018); LMA is a widely used indicator of different leaf anatomy and foliar structure strategies (Poorter et al., 2008); and tree height and dbh are indicators of tree structure and growth. Having access to measures of both leaf and structural (or physiognomic) traits for individual trees across the landscape potentially unlocks the ability to explore different dimensions of biodiversity together, investigate how these properties influence each other and affect competition among neighboring trees, and link to tree functions like growth and carbon exchange. However, exploring the links between leaf and structural traits across landscape is challenging, in part because of the differences in the design of their sampling approach.

Historically, structural traits are collected for thousands of trees in targeted areas via programs such as the US Forest Inventory and Analysis, whereas studies of leaf chemical traits have relied on collecting samples of a few leaves from a small number of individuals. These values are used to estimate the average trait values for each species and to explore how ecosystem level leaf traits vary biogeographically or through time by assuming that all individuals of a species in a region share the same trait value (Swenson et al., 2010, Clark et al., 2016). This approach is necessary because it is expensive and time consuming to collect individual level leaf trait data, but it fails to describe trait variation within species driven by evolution and plastic responses to the conditions an individual or population experiences (Messier et al., 2017, Niinemets et al, 2017, Muller et al. 2010, Nicotra et al. 2010, Albert et al. 2010, Callaway et al. 2003). Moreover,

since the number of leaf trait records is often orders of magnitude smaller than tree structural trait records, discrepancy in their sample size may affect the generality of relationships observed between leaf and structural traits at landscape scales. This limitation is magnified when studying changing environments (across space or time) because of bias in where the data for each species is collected. Data are typically collected in small subsets of the full range of conditions that species experience and are often selected in a biased manner that fits the purpose of the original studies (e.g., selecting individuals of a particular health status, size or species). Measuring traits systematically across geographic gradients would address this limitation, but is not feasible with traditional field methods (Anderson-Teixeira 2015).

An alternative approach that allows continuous estimation of traits across the landscape is to use remote sensing data (Kerr & Ostrovsky, 2003, Homolova et al. 2013, Houborg et al., 2015). For example, (a) hyperspectral remote sensing imagery is used to estimate the chemical composition of sunlit leaves by measuring light absorption and reflectance in the visible and near-infrared spectrum (Asner et al., 2017), and (b) light detection and ranging (LiDAR) is used to measure vertical and horizontal vegetation structure (Andersen et al., 2005). Leveraging remote sensing approaches allows for measuring trait information continuously at landscape scales. Together, LiDAR and hyperspectral data can be used to estimate many of the standard leaf and structural tree traits for trees (Serbin et al., 2014, Singh et al., 2015, Asner et al., 2017, Barbosa et al., 2017).

Traditionally, remote sensing applications use either the pixel (the smallest resolution component of the image, Audebert et al., 2019) or the plot (a region of space typically containing multiple individuals, Singh et al., 2015,) as the fundamental unit. This is a natural result of the structure of the remote sensing data combined with the difficulty of linking individual crowns in remote

105 sensing images to field data, especially for small crowns harder to detect with airborne
106 technology (Jakubowski et al., 2013). However, pixel or plot-based output results in a
107 disconnect between the remote sensing analysis and one of the fundamental biological units: the
108 individual (Liu et al., 2016, De Angelis, 2018, Marconi et al. 2019). Individual plants reproduce,
109 interact with their neighbors, and exhibit plastic responses to environmental conditions at the
110 individual scale. Populations of individuals evolve in response to natural selection. As a result,
111 our understanding of many biological processes is grounded in the individual and many field-
112 based survey methods focus on collecting data with individual trees as the primary unit of
113 measurement. While forest inventories hold information of the individual trees ineach plot
114 (Newnham et al., 2015), plot level estimates from remote sensing typically do not include
115 information about the relative distribution of individuals and their traits within the plot, thus
116 reducing the amount of information about community structure. To fully understand how traits
117 vary across space and time, and are determined by biological processes, it is important to
118 develop approaches linking these fundamental characteristics to individual trees in ways that can
119 be applied at scales of hundreds of km^2.

120 Despite its importance for biological research, few studies have attempted to model both leaf and
121 structural traits using remote sensing at the individual level over landscape scales (but see
122 Chadwick & Asner 2016, Martin et al., 2018). Even when crown level models are developed, the
123 resulting leaf trait predictions are made for pixels, not crowns, due to the challenges in crown
124 segmentation, poor spatial resolution of hyperspectral data, or misalignment between LiDAR and
125 hyperspectral data (Blaschke, 2010). Similarly, there are few studies estimating structural traits
126 (like crown height and area) at crown level, with traditional methods predicting tree height and
127 cover at the plot level (Kaartinen et al., 2012). Perhaps as a result of these differences, structural

and chemical leaf traits are not currently predicted together at large scales. Consequently, ecology lacks the large scale individual level trait estimates that are necessary to fully understand tradeoffs between leaf and tree structural traits, and to explore how trait variability relates to species and the environment. Data from NEON Airborne Observatory Platform NEON (AOP) provide co-registered, georeferenced, and atmospherically corrected high resolution hyperspectral data and LiDAR, whose integration represents a great opportunity to circumvent these challenges.

To address this gap, we developed a pipeline for making crown level trait predictions at scales of ~400 km^2 with associated uncertainties on both crown segmentation and trait estimation. Building on Chadwick & Asner (2016) and Martin et al. (2018), we: (1) identify individual crowns in remote sensing imagery that are associated with field-based trait measurements; (2) build models relating the remote sensing data to the field-based trait measurements; and (3) apply those models to estimate trait values and examine patterns of tree structural and chemical traits from individual to landscape scales. We advance the state of the art (Chadwick & Asner 2016, Martin et al. 2018) in this pipeline by using crown-level models and comparing them to pixel- and crown average-level models, directly estimating uncertainty in trait predictions using likelihoods, and predicting traits at the crown-level. Finally, derived data products on the location, size, shape, and leaf traits of millions of individual trees distributed over tens of thousands of hectares.

2. Methods

In our pipeline for predicting crown level leaf and structural traits from remote sensing we used: 1) field measurements of traits for building and evaluating models; 2) data on the shape and

location of individual tree crowns (ITCs) for building accurate models and assessing uncertainty in crown segmentation algorithms; and 3) high resolution remote sensing LiDAR (for crown segmentation and estimation of structural traits) and hyperspectral data (for estimation of leaf chemical traits). To obtain these components, we combined National Ecological Observatory Network's (NEON) airborne observatory data with field data we collected at NEON sites on leaf traits as well the location and shape of individual tree crowns.

2.1. Site descriptions

The study was conducted at two core terrestrial NEON sites; Ordway Swisher Biological Station in Florida (OSBS, NEON Domain 03) and the Oakmulgee Management District of Talladega National Forest in Alabama (TALL, NEON Doman 08). The two sites (Appendix S1: Figure S.1) have a mix of deciduous, evergreen, and mixed forest types (Homer et al., 2012). Upland areas at both sites are dominated by fire-tolerant oaks and pine species, primarily longleaf pine (*Pinus palustris*). The longleaf pine at OSBS forms open stands whereas the longleaf pine canopy at TALL is more closed. Lowland areas near lakes or wetlands (OSBS), and riparian areas (TALL) are dominated by closed canopy hardwood forests (Beckett and Golden 1982, Cox and Hart 2015).

2.2. Remote sensing data

All aerial remote sensing data products were provided by the NEON Airborne Observation Platform (NEON-AOP, Table 1). We used data from the May 2014 flight for OSBS, and the June 2015 flight for TALL. We used the raw L1 data products: (1) "classified LiDAR point cloud", and (2) "hyperspectral surface reflectance" data, orthorectified and atmospherically

171 corrected (details in data.neonscience.org/api/v0/documents/NEON.DOC.001288vA). To
172 reduce the effects of non-lambertian diffuse scattering, we applied the topographic and
173 bidirectional reflectance distribution function (BRDF) corrections by adapting scripts from the
174 HyTools repository (https://github.com/EnSpec/HyTools-sandbox) to our dataset. The LiDAR
175 data consist of 3D spatial point coordinates (4-6 points/m^2) which provides high resolution
176 information about crown shape and height. These data are released in 1 km x 1 km tiles.
177 Hyperspectral reflectance data consist of 1m^2 spatial resolution images with 426 channels (or
178 bands), each one collecting the magnitude of reflectance in 5 nm wide interval of wavelengths,
179 ranging from visible to near infrared light (from 350 to 2500 nm). These images were provided
180 as multiple ~15 km x 0.8 km flight lines with a total area of ~215 km^2 in OSBS, and ~145 km^2 in
181 TALL. The hyperspectral images were provided as "prototype" data, pre-processed differently
182 than post 2017 data, and delivered on hard drives. Prototype airborne data showed misalignments
183 between LiDAR and hyperspectral products, (as well as across hyperspectral flightpaths), on the
184 scale of 1-2 meters (Marconi et al. 2019, Appendix S1: Figure S.6), primarily affecting pixels at
185 crown borders. Despite the prototype data being potentially of lower quality than the newer
186 NEON AOP data, we used it to match the collection dates of the field data. The only difference
187 with current L1 and L3 data is in the nomenclature of the .h5 data structure, making the methods
188 presented here suitable with more recent NEON data.

189

190 *2.3.* Field Data

191 During this project, leaf trait data collected by the NEON Terrestrial Observation System (TOS)
192 were not available. Instead, we used a dataset of leaf samples collected for 157 trees, many of

193 which were near NEON inventory plots that are randomly located across the study site and
194 stratified by land cover type. The sampled trees were located away from major roads, had crowns
195 visible from airborne aircraft and identifiable in the image, and had sunlit branches that were
196 accessible for leaf collection. Trees were not sampled within NEON plots to avoid disturbing
197 NEON's long-term monitoring efforts. As wide a range of species as possible were collected,
198 including some rarer species that occured far from NEON plots (Appendix S1: Figure S.2).

199 Trait data were collected in the early part of the peak growing season in 2015. Specifically, 81
200 individual trees (of 17 species) were sampled from OSBS in May-June 2015, and 78 individuals
201 (26 species) in July 2015 from TALL. Leaves were sampled from the sunlit portion of the
202 canopy with a shotgun. Immediately after collection, the leaves were placed in a labeled plastic
203 bag and stored in a cooler until they could be processed in the field lab within 2-4 hours of
204 collection. The collected leaves were randomly sampled for further processing in two ways.
205 First, a sample of leaves (at least 20 grams of fresh leaves) was analyzed for nitrogen (%N),
206 carbon (%C), phosphorus (%P) by weight, according to standard protocols, with the exception
207 that petioles were removed (Murphy and Riley 1962; Cornelissen et al. 2003). Second, a sample
208 was processed for LMA using the Carnegie Institute for Science spectronomics protocol
209 (https://gao.asu.edu/spectranomics, Asner et al., 2011). Whole leaves were weighed then
210 scanned on a flatbed scanner to determine leaf area. The leaves were then dried at 60 C for at
211 least 72 hours and reweighed to get the dry leaf mass. For needle-leaf species, a sample of
212 individual needles (at least 3 fascicles per sample) was scanned and weighed. The needled
213 dimensions of a subset of the samples were also measured with calipers to calculate total surface
214 area. These measurements showed good agreement with the projected surface area from the

scans ($R^2 > 0.75$). This data and complete metadata will be added to TRY database v.6 (Kattge et al., 2020).

Individual trees were mapped in the remote sensing images using a field tablet and GIS software. Mapping was done on 2014 imagery for OSBS, and on 2015 imagery for TALL. This process involved mapping individual tree crowns on the hyperspectral image in the field to ensure the sampled trees matched directly with image pixels (Graves et al., 2018). This individual tree crown (ITC) data provides the most accurate link of field measurements with pixels from remote sensing spectral data and was used to quantify uncertainty in crown segmentation algorithms.

2.4. The algorithm pipeline

We developed a modular pipeline based on three steps: (1) build and evaluate crown segmentations from LiDAR data (section 2.6); (2) develop an ensemble of statistical models to infer leaf mass per area (LMA, g m^{-2}), nitrogen (%N), phosphorus (%P), and carbon (%C) per tree from hyperspectral data (section 2.5), and models to estimate structural traits [diameter at breast height, DBH (cm), crown area, CA (m^2) and stem height, H (m)] from LiDAR data; (3) make predictions for every individual tree crown in both NEON sites. For each crown, we also extracted values of elevation, slope and aspect provided as NEON AOP data products (Table 1), aiming to build a comprehensive dataset including topographic, leaf chemical and tree structural traits for any tree detected within the AOP footprint. We limited our analysis to individual tree crowns taller than 2 meters and wider than $1m^2$. Since the field traits dataset was for sunlit foliage, we predicted traits only from the upper portion of the canopy. The structure of the pipeline presented in this paper is summarized in Figure 1.

2.5. Leaf chemistry model

After correcting the hyperspectral data with the bidirectional reflectance distribution function and topographic correction, we extracted all pixels within the boundaries of the field-delineated ITCs. Shadowed or low vegetation pixels within the ITCs were removed using thresholds for both a near infrared band (reflectance in 860 nm < 0.3) and the Normalized Difference Vegetation Index (NDVI < 0.7) (Appendix S1: Figure S.3) Colgan et al., 2012, Graves et al., 2016). We normalized the spectral values for each pixel by dividing each spectral vector by its root sum of squares. We used this method to further reduce the effect of peripheral light and shadows within each crown (Singh et al., 2015, Feilhauer et al., 2010).

Field data were split at the tree level, and stratified by species, into training (n = 115), validation (n = 18), and test sets (n = 24). Since the two sites have similar species composition, we aggregated the two datasets to build a joint model. As is common for trait studies, our field data on foliar traits was averaged to a single value for each individual tree. Most algorithms require associating a single vector of predictor variables (i.e. the spectra) to a single response value (e.g. tree crown or plot). However, individual crowns contain multiple pixels, and crowns vary in the number and quality of these pixels. In each crown, some pixels will be better for linking traits to hyperspectral signatures because they reflect light primarily from leaves, whereas other pixels include reflectance from branches, understory, or ground. To address this, we used a bagging approach (Song et al., 2013) that takes advantage of different pixel characteristics by training, weighting, and ensembling models fit to different subsets of pixels. This approach weights the predictions from models fit to different pixels to produce a more generalizable and accurate representation of the relationship between foliar traits and their spectral signatures. To capture the range of possible models from different subsets of pixels in each crown, we randomly

sampled one pixel from each training crown 1000 times, and used the resulting 1000 vectors of pixels (one pixel for each crown in the dataset) to build 1000 independent partial least squares generalized linear regression (PLS-GLR) models (Bastien et al., 2005, Bertrand et al, 2014). Instead of the regular PLS regressions used in most trait modeling (e.g., Singh et al., 2015, Wang et al., 2020, Chadwick et al., 2018) we used PLS-GLR because it uses maximum likelihood estimation to calculate the regression parameters. This is an improvement over current approaches because it: (1) allows the calculation of AIC for model averaging (Burnham & Anderson 2002); (2) provides a robust measure of uncertainty in the form of a prediction interval (Christoffersen, 1998), which allows estimating the range of out of sample predictions rather than the range of mean response; and (3) does not require bootstrapping, making the method more scalable. We used a log-normal link function for all models to reflect the fact that all traits are positive numbers. We treated site (OSBS versus TALL) as a one hot encoder fixed effect (Harris & Harris, 2010) to account for site specific ancillary conditions. The number of components included in each model were determined using 5-fold cross-validation (CV) using the PRESS statistic (Tapley, 2000) on the training set. Models for each leaf trait were trained independently.

We compared four modeling strategies that varied in how the models were developed and how the models were applied for testing (Appendix S1: Table S.1). The models are labelled based on how the model was applied as “pixel based” (applied to individual pixels) or “crown based” (applied to segmented crowns). The models were built as follows: 1) a pixel-based approach with the spectra of a single pixel randomly extracted from each crown (SPM). This approach represents the case in which only the coordinates of the leaf sample are available, and spectral information can be extracted by sampling from a pixel corresponding to the stem or leaf location;

2) A pixel based approach (hereafter referred as the "ensemble pixel based model" (or EPBM) that included information on crown identity by labelling each pixel with an individual crown identifier and using it to ensemble a selection of 100 SPM models using multi-model averaging based on delta AIC (Burnham & Anderson 2002). In this step, we selected the 100 models for each trait that best performed on the independent validation dataset (n =15). This step was fundamental to: (a) drop models that performed worse than chance ($R^2 < 0$) and therefore held not meaningful relationships; (b) massively reduce the computational resources required to scale predictions to hundreds of km^2.This approach requires crown boundaries information for training but not for application, since it applies to individual pixels; 3) a simple crown average approach, hereafter "Crown Average Spectra" (CAS), where each individual tree was represented by the average of the spectra across all green pixels (i.e. pixels with NDVI >0.7 and NIR > 0.3) within the crown polygon; 4) A crown average approach, that we refer to as the "Crown Ensemble Aggregation Model" (CEAM), consisting on averaging predictions from the EPBM for all sunlit pixels belonging to individual tree crown polygons. We tested the performance of each approach in two ways, on pixels extracted from (1) ground delineated crowns (Graves et al., 2018), and (2) algorithmically delineated crowns (Silva et al., 2016). This step was fundamental to quantify the effect of uncertainty in crown detection and segmentation on predicting leaf traits at crown level across the landscape where no field delineated crowns are available.

All models were tested on the 24 crowns withheld in the test dataset. The test data were not used at any phase of the fitting or the ensemble process. Accuracy was evaluated using the predictive coefficient of determination (R^2) and the root-mean-square error (RMSE). The coefficient of determination produces values between 1 and negative infinity, where negative values indicate that the model predictability is lower than the sample average. As such, negative R^2 values

indicate that the statistical model did not learn any meaningful information from the data. A value of 1 indicates that predicted values perfectly match observations. We evaluated the uncertainty of predictions for each model using the coverage of the 95% prediction interval (95PI). The prediction interval is the range of values that is expected to contain 95% of the observed data points, and therefore a model with good estimates of uncertainty should have approximately 95% of the test data falling within this range. Since the CEAM was generated by the ensemble of the 100 best SPMs, we estimated the 95PI for CEAM predictions by averaging the error functions for the same 100 SPMs. We used the same data split, data transformation and PLS-GLR parameterization for all models. For pixel-based estimations (SPM and EPBM), we compared ground measures of LMA, N, C, and P with predictions from each pixel in the test dataset. For crown-based estimations (CAS and CEAM), we averaged pixel-based predictions belonging to all of the pixels in the crown. The same rationale was used for comparing pixel and crown-based uncertainty.

2.6. Tree structural traits and crown segmentation

We used the lidR R package (Roussel & Auty, 2017) to process point cloud LiDAR data to create a 0.5 m^2 resolution canopy height model (CHM) and produce algorithmically delineated crowns. Despite there was little difference to the $1m^2$ resolution of NEON CHM, we chose an higher resolution CHM to produce smoother polygons and leverage the information in regions where the point cloud was more dense. We used the CHM to determine the number of trees in the scene (i.e. tree detection) using local maxima filtering (Popesco et al., 2004). We tested three alternative methods for crown segmentation (Dalponte & Coomes 2016, Silva et al., 2016, and a watershed algorithm as in Barnes et al., 2014) and chose the best performing one to generate

crown boundaries (Appendix S1: Table S.2, Appendix S1: Section 1)**.** To evaluate accuracy of crown detection and segmentation on the targeted landscapes, we calculated: (1) an estimate of precision from all predicted crowns whose boundaries overlapped with the field ITCs; (2) pairwise Jaccard index coefficient (Real & Vargas, 1996), which represents the intersection over union between the areas of two polygons, and is the standard benchmarking metric for image analysis (Rezatofighi et al., The Jaccard index was calculated by comparing ITCs collected in the field with the single most overlapping predicted crown (Marconi et al., Field delineated crowns that do not overlap with any crown segmented by the algorithm were labelled as undetected. 2019). We estimated tree structural traits from the derived polygons and the CHM. Crown area (CA) was calculated from the polygon geometry using the geoPandas python package (https://geopandas.readthedocs.io/). Tree height (H) was extracted from the CHM as the maximum height within each ITC. Diameter at breast height (DBH) was calculated using an allometric regression model relating the log-transformed DBH taken from the NEON woody plant vegetation structure data to the log-transformed height and canopy area of the matching algorithmically delineated crowns for 566 individual stems. Delineated crowns were matched to field-mapped stems in the NEON dataset visually (Appendix S1: Table S.3).

2.7. Building individual-level derived data for full flight paths

Each remote sensing image was split into 1 km^2 tiles to optimize computational resources and allow parallelization on hundreds of cores. We pre-processed each tile using the same filters used for developing the models. To make predictions we used the EPBMs ensemble models to produce rasters of LMA, %C, %P and %N predictions and the 95PI for each suitable pixel and averaged them to crown level by using algorithmically delineated crowns. Crown-based predictions were achieved by averaging the values of all suitable pixels within the corresponding

predicted ITC boundaries. For those areas where the ITC overlapped with more than one flight path (flight paths overlap by ~30%), we averaged the crown-based predictions from both flight paths.

We stored flight-paths level maps of traits into raster data-products. The crown level dataset was then compiled as a comma delimited file containing all the geometry information to rebuild polygon shapes and locations. The data is distributed in a Zenodo archive (http://doi.org/10.5281/zenodo.3232978).

3. Results

We chose the crown segmentation algorithm described in Silva et al. (2016) (Appendix S1: Table S.2) to produce algorithmically delineated crowns. The approach detected ~88% of the field crowns (Appendix S1: Table S.5), but showed lower accuracy in estimating the shape and size of the canopies for individual trees, with Jaccard Index ranging between 0 (for undetected trees) and 0.81, with an average of 0.35. Crowns identified by the algorithm were generally larger than those delineated in the field, resulting in overestimated crown areas (especially for smaller trees) and weak correlations between field data and algorithmic crown areas (Figure 2). Low goodness of fit in predicting Crown Area (CA) was exacerbated by uncertainty in alignment with field and remote sensing data. For example, field crowns were delineated on the hyperspectral images to incorporate only the pure pixels of the crown (Graves et al., 2018, Appendix S1: Figure S.4, Appendix S1: Figure S.5) leading to potentially underestimating the full extent of tree crown size. Moreover, visual assessment of paired field and algorithmically delineated crowns shows shifts by 1-2 meters that likely result from imperfect alignment between LiDAR and hyperspectral data (Appendix S1: Figure S.6; Marconi et al. 2019), further

373 affecting uncertainty in field to algorithmically estimated crowns. Estimates of other structural
374 traits from the algorithmic tree crowns were better than crown area estimates. Height showed the
375 highest correspondence between field and remotely sensed measures (R^2 = 0.90 for trees higher
376 than 3m). Despite low accuracy in its predictions, CA showed a significant effect in estimating
377 DBH from LiDAR (Appendix S1: Table S.3). However, tree height was the most important
378 variable in predicting DBH, which therefore resulted in good estimates for both sites (0.62 R^2),
379 in the range of other recent applications (0.59 in Dalla Corte et al., 2020, 0.62 to 0.83 from Yao
380 et al., 2012).

381 We compared the four methods - two applied to pixels (the single pixel methods, SPM, and
382 ensemble pixel methods, EPBM) and two applied to crowns (the crown average, CAS and the
383 crown based ensemble methods, CEAM) - using RMSE. When tested on pixels extracted from
384 field delineated crowns, CEAM performed the best for %N and %P (RMSE of 0.20 and 0.026),
385 and CEAM and EPBM performed equivalently for LMA (RMSE of 40.3 and 40.8 respectively)
386 (Figure 3A, Appendix S1: Figure S.7). CEAM explained 75% of the variance in LMA, 66% of
387 the variance in %N, 46% of the variance in %P, and 41% of the variance in %C (Appendix S1:
388 Table S.4, Appendix S1: Figure S.8). These results were comparable to those obtained by Martin
389 et al. (2018) for trees in Borneo (71%, 46%, 44%, 48% respectively for LMA, %N, %P, %C).
390 Despite "site" ancillary information was an important feature for all models, its influence on
391 traits predictions was always relatively low compared to reflectance (as shown by the models'
392 parameters, Appendix S1: Figure S.9). The root mean squared error (normalized by traits
393 observations range, NRMSE) was always between 8 and 16% of the range of the field
394 observations, meeting the quality threshold recommended by Singh et al. (2015).

The ensemble approaches (CEAM and EPBM) performed better than methods based on pixels as the fundamental unit (SPM) or simple averaging of all green pixels in a crown (CAS) when the assessment was on field delineated crowns (Appendix S1: Table S.4; Figure 3A). Few individual SPMs performed better than the EPBM ensembles (Appendix S1: Figure S.10) and when individual pixel models did outperform the ensemble, they usually were not among the best SPM models (i.e., the models with the lowest delta AIC in the validation). This suggests that EPBM provides the best method for making out-of-sample predictions at the pixel level. CEAM generally produced the best estimates of uncertainty. CEAM 95PI showed an average coverage of 95% of held out observations, CAS 94%, EPSM 91%, Plot and SBM 90%, with the ideal value being 95% (Figure 3D).

The CEAM approach performed best when making predictions using pixels extracted from algorithmically delineated crowns (Figure 3). Compared to when crown boundaries are collected from the field, the accuracy of predictions using algorithmically delineated crowns was reduced due to the uncertainty associated with crown segmentation. However, CEAM showed the lowest reduction in accuracy compared to the other approaches (ΔNRMSE ~ 2%, Figure 3C), resulting in the lowest NRMSE for all traits (Figure 3B).

Scaling algorithmic crown segmentation and trait estimation to the full extent of the NEON remote sensing data yielded trait predictions for approximately 5 million canopy trees for the two sites combined (Figure 4, Appendix S1: Figure S.11, S.12, S.13). Landscape patterns in traits are evident, including east-west gradients in LMA, %N, and %P at OSBS (Figure 4). At TALL, lower LMA and higher %N and %P are found in a dendritic pattern associated with the stream network (Appendix S1: Figure S.12). Some traits show a bimodal distribution at each site, which is probably related to differences in needleleaf versus broadleaf species but would need to be

418 further tested with trait estimation coupled with species predictions. On average, OSBS showed
419 higher %N and %P compared to TALL (Figure 5). Distributions of LMA, %N, and %P in OSBS
420 shifted to higher values than TALL, following patterns observed from the field data (Figure 5,
421 Appendix S1: Figure S.15). Assessing correlations between estimated structural traits, leaf traits,
422 and abiotic environmental conditions showed strong correlations between LMA, %N, and %P,
423 consistent with the leaf economic spectrum (Wright et al., 2004) (Appendix S1: Figure S.14). Of
424 the environmental variables, elevation had the strongest relationship with leaf traits with leaf N
425 and P decreasing and LMA increasing with elevation (Figures S.15, S.16). Leaf traits and tree
426 structure were correlated at OSBS (e.g. LMA with tree H, figure 5B) but not TALL.

427 # 4. Discussion

428 The individual organism is one of the fundamental units of biology. As a result, studying the
429 distribution of individuals and their traits across space and through time is central to many
430 aspects of ecology. However, collecting individual level data at the large scales required for
431 many ecological questions is challenging. To address this limitation we develop a fully
432 automated modular pipeline to link remote sensing products from the National Ecological
433 Observatory Network (NEON) to data collected in the field, convert the remote sensing data into
434 estimates of the leaf and structural traits for all canopy trees detected at landscape scales, and
435 estimate the traits for millions of individual trees in an open and accessible format (Cassey et al.,
436 2006, Hampton et al., 2016) for use by the broader scientific community.

437 We found that modeling and predicting leaf traits at the individual crown level resulted in
438 improved accuracy and uncertainty in the predictions compared to pixel based approaches
439 (Figure 3). Linking pixels to crowns allows the ensembling of models built from the different

pixels making up the crowns. Different pixels contain different combinations of leaves, branches, understory and ground, which affects the underlying chemometric relationship between foliar traits and their spectral signature. Weighted ensembling provides one way to address this, by allowing the models to identify the best combinations of pixels for relating traits and hyperspectral signatures. Aggregating pixel predictions to the crown level may also reduce the influence of outlier pixels. Our method produced models with predictive power comparable to two other crown-based estimation methods (Barbosa and Asner, 2017; Martin et al., 2018), suggesting that the performance of these approaches may generalize beyond the current study. In addition to providing robust leaf trait estimates, crown level methods allow the simultaneous estimation of structural traits, allowing these two sets of traits to be analyzed together at large scales.

2019). This is likely because height is directly measured by LIDAR and height was the most important factor in the allometric models used to predict DBH. 2018, Jucker et al. 2016). While our crown-based methods were effective for estimating a number of leaf and structural traits, there is substantial uncertainty even for the best performing traits. Quantifying this uncertainty provides information on the range of likely trait values for each individual and allows this uncertainty to be propagated when using these derived data values to test scientific hypotheses (Miller-Gulland and Shea, 2017). We used methods for leaf trait estimation that allowed us to estimate uncertainty (pls-GLR) and the crown-based method (CEAM) provided the best uncertainty estimates (Figure 3, Appendix S1: Table S.4). Current methods for delineating crowns do not include explicit measures of uncertainty (Dalponte & Coomes 2016, Silva et al., 2016). It is important for future methods to address this limitation because comparisons to field data suggested high uncertainty in segmentation.

463 One of the challenges for crown level approaches is that they rely on crown segmentation
464 algorithms to identify the location and size of individual trees. While we used the best
465 performing crown segmentation the algorithm from a recent methods competition (Marconi et al.
466 2019) and had reasonable correspondence between the presence of an algorithmic crown and
467 each field crown, the algorithmic crowns averaged only 35% overlap in area with the most
468 similar field delineated crown. Heterogeneity in point cloud density and misalignment between
469 lidar and hyperspectral sensors could contribute to misalignment between field and
470 algorithmically delineated crowns (Marconi et al, 2019, Kamoske et al., 2019, Appendix S1:
471 Section 1). Despite this uncertainty, estimates of DBH and height were well correlated with field
472 values.Therefore data derived from our pipeline should be useful for assessing estimates of
473 individual tree biomass by applying allometric functions linking biomass to DBH and height
474 (Graves et al. Crown area was more susceptible to the segmentation uncertainty, but is also more
475 sensitive to small errors in segmentation and CHM resolution (Appendix S1: Section 1).

476 Uncertainty in crown segmentation can also have cascading impacts on the estimation of leaf
477 traits, which was tested by comparing results from field versus algorithmically delineated tree
478 crowns. Prediction accuracy is generally lower when using algorithmically delineated crowns
479 because the pixels used for making predictions both include pixels that are not in the true crown
480 and exclude pixels that are in the true crown. However, these decreases in accuracy were
481 generally quite small, with decreases in NRMSE of <0.05 across all methods. The crown-based
482 ensemble method (CEAM) was particularly robust to this uncertainty, with the smallest increases
483 in NRMSE and all traits maintaining NRMSE below Singh et al. (2015)'s threshold (Figure 3C,
484 Appendix S1: Table S.4). This robustness may result because the weighted ensembles in CEAM

485 provide the ability to weight pixels algorithmically, allowing it to ignore pixels from outside of
486 the true crown.

487 Generating derived individual level data on leaf and structural traits at the landscape scale allows
488 trait patterns at these scales to be effectively assessed. While a complete analysis of the spatial
489 distribution of tree traits is beyond the scope of this paper, our results showed some general
490 patterns worth future investigations. LMA, %N, and %C showed bimodal distributions at both
491 sites (with %N peaks particularly close in OSBS), likely because pines and oaks, the most
492 common needleaf and broadleaf genera respectively at these two sites, occupy distinct regions of
493 the worldwide Leaf Economic Spectrum (LES)(Wright et al., 2004). Correlation patterns
494 between LMA and %N, %N and %P, and LMA and %P match the global scale patterns observed
495 globally in the LES. Despite the limited number of species and geographical extent, both sites
496 showed rangeand spread of LMA, %N and %P overlapping with most of the global range of the
497 worldwide LES tradeoffs (Appendix S1: Figure S.14). This suggests that variation in the local
498 environment could be driving large intra-species variability of leaf traits, while conserving the
499 general trade-offs observed across species (Asner et al., 2016). Among the environmental
500 variables we tested, elevation showed the strongest correlation with leaf traits (Appendix S1:
501 Figure S.16, Appendix S1: Figure S. 17), possibly because elevation represents a proxy of
502 different soil conditions in these sites, which can affect both species distributions and leaf traits
503 (Walter & Gerlach, 2013). For example, small differences in elevation at OSBS often means
504 transitioning from drained sandhill (that favor pines) to marshy and richer soils that favor the
505 establishment of large-crowned broadleaf species, rich in foliar %N and %P (Bodker et al.,
506 2015).

Producing derived data at the individual level also facilitates landscape scale assessments of relationships between leaf and structural traits at the level of individual organisms. For example, although the two sites have similar species composition, our results showed different correlational patterns between structural (height and DBH) and chemical traits (LMA, %N, %P, %C) (Figure 5, Appendix S1: Figure S.17), especially the relationship between height and LMA ($r = 0.24$ in OSBS, $r = -0.08$ in TALL). Possible explanations for these relationships may be related to differences in management histories across patches of the landscape that can influence species assembly, successional stages, which are important determinants of tree size and leaf traits (Sameulson and Stokes 2012; Ishida et al. 2005). Our pipeline, integrated with further remote sensing derived information (e.g. species identities) and local history (e.g. management and fire history) could be used to address how these drivers affect local distribution of plant traits, their trade-offs, and their effects on the ecosystems across a multitude of landscapes.

Our crown-based approach to modeling and predicting tree traits produces individual data similar to that collected in the field. This approach has a number of benefits. First, it will make data integration with field-based forest and trait surveys easier because both derived remote sensing data and field surveys will be composed of the same fundamental unit (individual trees). Second, crown-based approaches are likely better for aligning trait data across years. The same pixel in two consecutive years could vary significantly in a trait because of small errors in spatial alignment of pixels through time, whereas large crown-level regions will be more robust to small errors at the edges of the crown. Moreover, multi-temporal and multi-sensor images can be potentially leveraged to align and improve segmentation for crown objects captured in the same scene (Bovolo & Buzzone, 2017, Sumbul et al., 2020). Finally, this approach allows a more compact representation of derived trait data in tabular formas spatial polygons instead of rasters.

While this will not be the best representation for all analyses, for individual level analyses it results in vastly reduced storage computational requirements compared to raster data.

Thanks to the modular nature of our approach, crown segmentation can easily be substituted with methods based on RGB (Weinstein et al., 2020) or hyperspectral imaging (Dalponte et al., 2016) when LiDAR data is poor or not available. Yet, individual level approaches are limited by data availability and are not suitable for addressing ecological questions at continental to global scale. High resolution airborne remote sensing is still limited to relatively few sites, while the resolution of AVIRIS or satellite data is more appropriate for plot level analyses (e.g., Singh et al. 2015, Martin et al. 2018, Ma et al. 2019). However, these two approaches can be potentially integrated to scale sub-pixel properties from satellite data, and merge the gap between local, regional and global scale ecological information, and better address emergent cross-scale ecological questions related to variation of leaf traits, diversity and functions (Carmona et al., 2016).

The data produced by our individual level pipeline could be extended by including predictions for species identity, other leaf and structural traits, environmental variables, management, or disturbance. Moreover, our pipeline can potentially be used to extract ecological information for every tree that can be detected across all NEON AOP sites for the full life of the observatory. This will produce a publicly available, spatially explicit database of detailed ecological information for hundreds of millions of trees across the US that could be fused with other continental data (e.g. Forest Inventory and Analysis) and integrated to area based analyses from satellite data, to address cross scale functional ecological questions (http://doi.org/10.5281/zenodo.3232978). Such data could be used to further understand the

552 biology behind trait tradeoffs and investigate cross scale ecological processes and patterns from
553 individual to landscape to continental scale.

554 5. *Acknowledgments*

555 This work was supported by the Gordon and Betty Moore Foundation's Data-Driven Discovery
556 Initiative through grant GBMF4563 to E.P. White and by the National Science Foundation
557 through grant 1926542 to E.P. White, S.A. Bohlman, A. Zare, D.Z. Wang, and A. Singh; by the
558 NSF Dimension of Biodiversity program grant (DEB-1442280) and USDA/NIFA McIntire-
559 Stennis program (FLA-FOR-005470) to S. A. Bohlman; by the University of Florida
560 Biodiversity Institute (UFBI) and Informatics Institute (UFII) Graduate Fellowship to Sergio
561 Marconi. There was no additional external funding received for this study.

562

563 6. *Description of author's responsibilities*

564

565 Sergio Marconi and Sarah Graves designed the experiment, Sarah Graves carried out field work,
566 Sergio Marcon, Sarah Graves and Ethan White developed the methods, Sergio Marconi
567 performed the analysis, Ethan White and Stephanie Bohlman supervised the work as lab leaders,
568 helped with experimental design and advice on data analysis. Ben Weinstein helped with
569 technical aspects and manuscript editing. All authors contributed to editing the manuscript. We
570 acknowledge Dr. Adytia Singh for his suggestions in the initial phase of the project, and the
571 reviewers that contributed to significantly improve this manuscript.

572

References

1. Albert, C.H., Thuiller, W., Yoccoz, N.G., Soudant, A., Boucher, F., Saccone, P. and Lavorel, S., 2010. Intraspecific functional variability: extent, structure and sources of variation. Journal of Ecology, 98(3), pp.604-613.

2. Andersen, H.E., McGaughey, R.J. and Reutebuch, S.E., 2005. Estimating forest canopy fuel parameters using LIDAR data. Remote sensing of Environment, 94(4), pp.441-449.

3. Anderson□Teixeira, K.J., Davies, S.J., Bennett, A.C., Gonzalez□Akre, E.B., Muller□Landau, H.C., Joseph Wright, S., Abu Salim, K., Almeyda Zambrano, A.M., Alonso, A., Baltzer, J.L. and Basset, Y., 2015. CTFS□ForestGEO: a worldwide network monitoring forests in an era of global change. Global change biology, 21(2), pp.528-549.

1. Asner, G.P., Martin, R.E., Knapp, D.E., Tupayachi, R., Anderson, C.B., Sinca, F., Vaughn, N.R. and Llactayo, W., 2017. Airborne laser-guided imaging spectroscopy to map forest trait diversity and guide conservation. Science, 355(6323), pp.385-389.

4. Asner, G.P., Knapp, D.E., Anderson, C.B., Martin, R.E. and Vaughn, N., 2016. Large-scale climatic and geophysical controls on the leaf economics spectrum. Proceedings of the National Academy of Sciences, 113(28), pp.E4043-E4051.

5. Asner, G. P., Martin, R. E., Tupayachi, R., Emerson, R., Martinez, P., Sinca, F., ... & Lugo, A. E. (2011). Taxonomy and remote sensing of leaf mass per area (LMA) in humid tropical forests. Ecological Applications, 21(1), 85-98.

592 6. Audebert, B. Le Saux and S. Lefevre, "Deep Learning for Classification of Hyperspectral
593 Data: A Comparative Review," in IEEE Geoscience and Remote Sensing Magazine, vol.
594 7, no. 2, pp. 159-173, June 2019, doi: 10.1109/MGRS.2019.2912563.

595 7. Bannister, J.M., Herbert, E.R. and Craft, C.B., 2015. Spatial variability in sedimentation,
596 carbon sequestration, and nutrient accumulation in an alluvial floodplain forest. In The
597 Role of Natural and Constructed Wetlands in Nutrient Cycling and Retention on the
598 Landscape (pp. 41-55). Springer, Cham.

599 8. Barbosa, J.M. and Asner, G.P., 2017. Prioritizing landscapes for restoration based on
600 spatial patterns of ecosystem controls and plant–plant interactions. Journal of Applied
601 Ecology, 54(5), pp.1459-1468.

602 9. Barnes, R., Lehman, C., Mulla, D., 2014. Priority-flood: An optimal depression-filling
603 and watershed-labeling algorithm for digital elevation models. Computers & Geosciences
604 62, 117–127. doi:10.1016/j.cageo.2013.04.024

605 10. Bastien, P., Vinzi, V.E. and Tenenhaus, M., 2005. PLS generalised linear regression.
606 Computational Statistics & data analysis, 48(1), pp.17-46.

607 11. Blaschke, T., 2010. Object based image analysis for remote sensing. ISPRS journal of
608 photogrammetry and remote sensing, 65(1), pp.2-16.

609 2. Bodker, J.E., Turner, R.E., Tweel, A., Schulz, C. and Swarzenski, C., 2015. Nutrient-
610 enhanced decomposition of plant biomass in a freshwater wetland. Aquatic Botany, 127,
611 pp.44-52.

612 12. M. Han, Y., Bovolo, F. and Bruzzone, L., 2017. Segmentation-based fine registration of
613 very high resolution multitemporal images. IEEE Transactions on Geoscience and
614 Remote Sensing, 55(5), pp.2884-2897.

615 13. Callaway, R.M., Pennings, S.C. and Richards, C.L., 2003. Phenotypic plasticity and
616 interactions among plants. Ecology, 84(5), pp.1115-1128.

617 14. Carmona, C.P., De Bello, F., Mason, N.W. and Lepš, J., 2016. Traits without borders:
618 integrating functional diversity across scales. Trends in ecology & evolution, 31(5),
619 pp.382-394.

620 15. Cassey, P. and Blackburn, T.M., 2006. Reproducibility and repeatability in ecology.
621 BioScience, 56(12), pp.958-959.

622 16. Chadwick, K.D. and Asner, G.P., 2016. Organismic-scale remote sensing of canopy
623 foliar traits in lowland tropical forests. Remote Sensing, 8(2), p.87.

624 17. Christoffersen, P.F., 1998. Evaluating interval forecasts. International economic review,
625 pp.841-862.

626 18. Clark, J.S., Gelfand, A.E., Woodall, C.W. and Zhu, K., 2014. More than the sum of the
627 parts: forest climate response from joint species distribution models. Ecological
628 Applications, 24(5), pp.990-999.

629 19. Clark, J.S., 2016. Why species tell more about traits than traits about species: predictive
630 analysis. Ecology, 97(8), pp.1979-1993.

631 20. Colgan, M.S., Baldeck, C.A., Féret, J.B. and Asner, G.P., 2012. Mapping savanna tree
632 species at ecosystem scales using support vector machine classification and BRDF

633 correction on airborne hyperspectral and LiDAR data. Remote Sensing, 4(11), pp.3462-
634 3480.

635 21. Collalti, A., P. E. Thornton, A. Cescatti, A. Rita, M. Borghetti, A. Nole, C. Trotta, P.
636 Ciais, and G. Matteucci., 2019. The sensitivity of the forest carbon budget shifts across
637 processes along with stand development and climate change. Ecological Applications
638 00(0): e01837. 10.1002/eap.1837

639 22. Cornelissen, J. H. C., S. Lavorel, E. Garnier, S. Diaz, N. Buchmann, D. E. Gurvich, P. B.
640 Reich, H. ter Steege, H. D. Morgan, M. G. A. van der Heijden, J. G. Pausas, and H.
641 Poorter. 2003. A handbook of protocols for standardised and easy measurement of plant
642 functional traits worldwide. Australian Journal of Botany 51:335 – 380.

643 23. Dalponte, M. and Coomes, D.A., 2016. Tree□centric mapping of forest carbon density
644 from airborne laser scanning and hyperspectral data. Methods in ecology and evolution,
645 7(10), pp.1236-1245.

646 24. De Angelis, D.L., 2018. Individual-based models and approaches in ecology:
647 populations, communities and ecosystems. CRC Press.

648 25. Diaz et al, 2016, The global spectrum of plant form and function. Nature 529:167–171.
649 10.1038/nature16489.

650 26. Dwyer, J.M. and Laughlin, D.C., 2017. Constraints on trait combinations explain climatic
651 drivers of biodiversity: The importance of trait covariance in community assembly.
652 Ecology letters, 20(7), pp.872-882.

27. Feilhauer, H., Asner, G.P. and Martin, R.E., 2015. Multi-method ensemble selection of spectral bands related to leaf biochemistry. Remote Sensing of Environment, 164, pp.57-65.

28. Frederic Bertrand, Nicolas Meyer and Myriam Maumy-Bertrand (2014). Partial Least Squares Regression for Generalized Linear Models, R package version 1.1.1.

29. Graves, S.J., Caughlin, T.T., Asner, G.P. and Bohlman, S.A., 2018. A tree-based approach to biomass estimation from remote sensing data in a tropical agricultural landscape. Remote sensing of environment, 218, pp.32-43.

30. Graves, S.J., Asner, G.P., Martin, R.E., Anderson, C.B., Colgan, M.S., Kalantari, L. and Bohlman, S.A., 2016. Tree species abundance predictions in a tropical agricultural landscape with a supervised classification model and imbalanced data. Remote Sensing, 8(2), p.161.

31. Graves S, Gearhart J, Caughlin TT, Bohlman S. 2018. A digital mapping method for linking high-resolution remote sensing images to individual tree crowns. PeerJ Preprints6:e27182v1 https://doi.org/10.7287/peerj.preprints.27182v1

32. Hampton, S.E., Anderson, S.S., Bagby, S.C., Gries, C., Han, X., Hart, E.M., Jones, M.B., Lenhardt, W.C., MacDonald, A., Michener, W.K. and Mudge, J., 2015. The Tao of open science for ecology. Ecosphere, 6(7), pp.1-13.

33. Harris, D. and Harris, S., 2010. Digital design and computer architecture. Morgan Kaufmann.

673 34. Houborg, R., Fisher, J.B. and Skidmore, A.K., 2015. Advances in remote sensing of
674 vegetation function and traits.

675 35. Jakubowski,K., Q. Guo, and M. Kelly. 2013. Tradeoffs between lidar pulse density and
676 forest measurement accuracy. Remote Sensing of Environment 130:245–253.

677 36. Jucker, T., Avăcări ei, D., Bărnoaiea, I., Duduman, G., Bouriaud, O. and Coomes, D.A.,
678 2016. Climate modulates the effects of tree diversity on forest productivity. Journal of
679 Ecology, 104(2), pp.388-398.

680 3. Kaartinen, H., Hyyppä, J., Yu, X., Vastaranta, M., Hyyppä, H., Kukko, A., Holopainen,
681 M., Heipke, C., Hirschmugl, M., Morsdorf, F. and Næsset, E., 2012. An international
682 comparison of individual tree detection and extraction using airborne laser
683 scanning. Remote Sensing, 4(4), pp.950-974.

684 37. Kamoske, A.G., Dahlin, K.M., Stark, S.C. and Serbin, S.P., 2019. Leaf area density from
685 airborne LiDAR: Comparing sensors and resolutions in a temperate broadleaf forest
686 ecosystem. Forest Ecology and Management, 433, pp.364-375.

687 38. Kattge, J., Bönisch, G., Díaz, S., Lavorel, S., Prentice, I.C., Leadley, P., Tautenhahn, S.,
688 Werner, G.D., Aakala, T., Abedi, M. and Acosta, A.T., 2020. TRY plant trait database–
689 enhanced coverage and open access. Global change biology, 26(1), pp.119-188.

690 39. Lawler, J.J., Tear, T.H., Pyke, C., Shaw, M.R., Gonzalez, P., Kareiva, P., Hansen, L.,
691 Hannah, L., Klausmeyer, K., Aldous, A. and Bienz, C., 2010. Resource management in a
692 changing and uncertain climate. Frontiers in Ecology and the Environment, 8(1), pp.35-
693 43.

694 40. Li, X., Messina, J.P., Moore, N.J., Fan, P. and Shortridge, A.M., 2017. MODIS land
695 cover uncertainty in regional climate simulations. Climate Dynamics, 49(11-12),
696 pp.4047-4059.

697 41. Liu, X., Swenson, N.G., Lin, D., Mi, X., Umaña, M.N., Schmid, B. and Ma, K., 2016.
698 Linking individual□level functional traits to tree growth in a subtropical forest. Ecology,
699 97(9), pp.2396-2405.

700 42. Ma, X., Mahecha, M.D., Migliavacca, M., van der Plas, F., Benavides, R., Ratcliffe, S.,
701 Kattge, J., Richter, R., Musavi, T., Baeten, L. and Barnoaiea, I., 2019. Inferring plant
702 functional diversity from space: the potential of Sentinel-2. Remote Sensing of
703 Environment, 233, p.111368.

704 43. Marconi, S., Graves, S.J., Gong, D., Nia, M.S., Le Bras, M., Dorr, B.J., Fontana, P.,
705 Gearhart, J., Greenberg, C., Harris, D.J. and Kumar, S.A., 2018. A data science challenge
706 for converting airborne remote sensing data into ecological information (No. e26966v1).
707 PeerJ Preprints.

708 44. Martin, M. E., L. C. Plourde, S. V. Ollinger, M. L. Smith, and B. E. McNeil. 2008. A
709 generalizable method for remote sensing of canopy nitrogen across a wide range of forest
710 ecosystems. Remote Sensing of Environment 112:3511–3519.

711 45. Martin, R.E., Chadwick, K.D., Brodrick, P.G., Carranza-Jimenez, L., Vaughn, N.R. and
712 Asner, G.P., 2018. An approach for foliar trait retrieval from airborne imaging
713 spectroscopy of tropical Forests. Remote Sensing, 10(2), p.199.

714 46. McGill, B.J., Enquist, B.J., Weiher, E. and Westoby, M., 2006. Rebuilding community
715 ecology from functional traits. Trends in ecology & evolution, 21(4), pp.178-185.

716 47. Messier, J., McGill, B.J., Enquist, B.J. and Lechowicz, M.J., 2017. Trait variation and
717 integration across scales: is the leaf economic spectrum present at local scales?.
718 Ecography, 40(6), pp.685-697.

719 48. Milner□Gulland, E.J. and Shea, K., 2017. Embracing uncertainty in applied ecology.
720 Journal of applied ecology, 54(6), pp.2063-2068.

721 49. Müller, I., Schmid, B. and Weiner, J., 2000. The effect of nutrient availability on biomass
722 allocation patterns in 27 species of herbaceous plants. Perspectives in plant ecology,
723 evolution and systematics, 3(2), pp.115-127.

724 50. Murphy, J., and J. P. Riley. 1962. A modified single solution method for the
725 determination of phosphate in natural waters. Analytica Chimica Acta 27:31 – 36.

726 51. National Ecological Observatory Network. 2014. Data Products NEON.DP1.10098,
727 NEON.DP1.30010, NEON.DP3.30015, NEON.DP1.30008. Provisional data
728 downloaded from http://data.neonscience.org on 26 Jan 2016. Battelle, Boulder, CO,
729 USA

730 52. Newnham, G.J., Armston, J.D., Calders, K., Disney, M.I., Lovell, J.L., Schaaf, C.B.,
731 Strahler, A.H. and Danson, F.M., 2015. Terrestrial laser scanning for plot-scale forest
732 measurement. Current Forestry Reports, 1(4), pp.239-251.

733 53. Nicotra, A.B., Atkin, O.K., Bonser, S.P., Davidson, A.M., Finnegan, E.J., Mathesius, U.,
734 Poot, P., Purugganan, M.D., Richards, C.L., Valladares, F. and van Kleunen, M., 2010.

735 Plant phenotypic plasticity in a changing climate. Trends in plant science, 15(12), pp.684-
736 692.

737 54. Niinemets, Ü., Keenan, T.F. and Hallik, L., 2015. A worldwide analysis of
738 within□canopy variations in leaf structural, chemical and physiological traits across plant
739 functional types. New Phytologist, 205(3), pp.973-993.

740 55. Nock, C. A., Vogt, R. J. and Beisner, B. E. (2016). Functional Traits. In eLS, John Wiley
741 & Sons, Ltd (Ed.). doi:10.1002/9780470015902.a0026282

742 56. Pollock, L.J., Morris, W.K. and Vesk, P.A., 2012. The role of functional traits in species
743 distributions revealed through a hierarchical model. Ecography, 35(8), pp.716-725.

744 57. Popescu, Sorin & Wynne, Randolph. (2004). Seeing the Trees in the Forest: Using Lidar
745 and Multispectral Data Fusion with Local Filtering and Variable Window Size for
746 Estimating Tree Height. Photogrammetric Engineering and Remote Sensing. 70. 589-
747 604. 10.14358/PERS.70.5.589.

748 58. Poorter, H., Niinemets, Ü., Poorter, L., Wright, I.J. and Villar, R., 2009. Causes and
749 consequences of variation in leaf mass per area (LMA): a meta□analysis. New
750 phytologist, 182(3), pp.565-588.

751 59. Prado-Junior, J.A., Schiavini, I., Vale, V.S., Raymundo, D., Lopes, S.F. and Poorter, L.,
752 2016. Functional traits shape size-dependent growth and mortality rates of dry forest tree
753 species. Journal of Plant Ecology, 10(6), pp.895-906.

754 60. Real, R. and Vargas, J.M., 1996. The probabilistic basis of Jaccard's index of similarity.
755 Systematic biology, 45(3), pp.380-385.

61. Rezatofighi, H., Tsoi, N., Gwak, J., Sadeghian, A., Reid, I. and Savarese, S., 2019. Generalized intersection over union: A metric and a loss for bounding box regression. In Proceedings of the IEEE Conference on Computer Vision and Pattern Recognition (pp. 658-666).

62. Roussel, J.R. and Auty, D., 2017. lidR: Airborne LiDAR Data Manipulation and Visualization for Forestry Applications.

63. Sarstedt, M., Hair, J.F., Ringle, C.M., Thiele, K.O. and Gudergan, S.P., 2016. Estimation issues with PLS and CBSEM: Where the bias lies!. Journal of Business Research, 69(10), pp.3998-4010.

64. Sexton, J.O., Noojipady, P., Anand, A., Song, X.P., McMahon, S., Huang, C., Feng, M., Channan, S. and Townshend, J.R., 2015. A model for the propagation of uncertainty from continuous estimates of tree cover to categorical forest cover and change. Remote Sensing of Environment, 156, pp.418-425.

65. Silva, C.A., Hudak, A.T., Vierling, L.A., Loudermilk, E.L., O'Brien, J.J., Hiers, J.K., Jack, S.B., Gonzalez-Benecke, C., Lee, H., Falkowski, M.J. and Khosravipour, A., 2016. Imputation of individual Longleaf Pine (Pinus palustris Mill.) Tree attributes from field and LiDAR data. Canadian journal of remote sensing, 42(5), pp.554-573.

66. Singh, A., Serbin, S.P., McNeil, B.E., Kingdon, C.C. and Townsend, P.A., 2015. Imaging spectroscopy algorithms for mapping canopy foliar chemical and morphological traits and their uncertainties. Ecological Applications, 25(8), pp.2180-2197.

776 67. Song, L., Langfelder, P. and Horvath, S., 2013. Random generalized linear model: a
777 highly accurate and interpretable ensemble predictor. BMC bioinformatics, 14(1), p.5.

778 68. Sumbul, G., Cinbis, R.G. and Aksoy, S., 2019. Multisource region attention network for
779 fine-grained object recognition in remote sensing imagery. IEEE Transactions on
780 Geoscience and Remote Sensing, 57(7), pp.4929-4937.

781 69. Swenson, N.G. and Weiser, M.D., 2010. Plant geography upon the basis of functional
782 traits: an example from eastern North American trees. Ecology, 91(8), pp.2234-2241.

783 70. Tarpey, T., 2000. A note on the prediction sum of squares statistic for restricted least
784 squares. The American Statistician, 54(2), pp.116-118.

785 71. Tang, Z., Xu, W., Zhou, G., Bai, Y., Li, J., Tang, X., Chen, D., Liu, Q., Ma, W., Xiong,
786 G. and He, H., 2018. Patterns of plant carbon, nitrogen, and phosphorus concentration in
787 relation to productivity in China's terrestrial ecosystems. Proceedings of the National
788 Academy of Sciences, 115(16), pp.4033-4038.

789 72. Valladares, F., Matesanz, S., Guilhaumon, F., Araújo, M.B., Balaguer, L.,
790 Benito□Garzón, M., Cornwell, W., Gianoli, E., Kleunen, M., Naya, D.E. and Nicotra,
791 A.B., 2014. The effects of phenotypic plasticity and local adaptation on forecasts of
792 species range shifts under climate change. Ecology letters, 17(11), pp.1351-1364.

793 73. Varner, J. Morgan, et al. "Post-fire tree stress and growth following smoldering duff
794 fires." Forest Ecology and Management 258.11 (2009): 2467-2474.

74. Walters, Michael B., and John P. Gerlach. "Intraspecific growth and functional leaf trait responses to natural soil resource gradients for conifer species with contrasting leaf habit." Tree physiology 33.3 (2013): 297-310.

75. Weinstein, B., Marconi, S., Bohlman, S., Zare, A. and White, E., 2019. Individual tree-crown detection in RGB imagery using self-supervised deep learning neural networks. bioRxiv, p.532952.

76. Wright, I.J., Reich, P.B., Westoby, M., Ackerly, D.D., Baruch, Z., Bongers, F., Cavender-Bares, J., Chapin, T., Cornelissen, J.H., Diemer, M. and Flexas, J., 2004. The worldwide leaf economics spectrum. Nature, 428(6985), p.821.

77. Yang, J., Cao, M. and Swenson, N.G., 2018. Why functional traits do not predict tree demographic rates. Trends in ecology & evolution, 33(5), pp.326-336.

78. Yao, W., Krzystek, P. and Heurich, M., 2012. Tree species classification and estimation of stem volume and DBH based on single tree extraction by exploiting airborne full-waveform LiDAR data. Remote Sensing of Environment, 123, pp.368-380.

79. Zhen, Z., Quackenbush, L.J. and Zhang, L., 2016. Trends in automatic individual tree crown detection and delineation—evolution of lidar data. Remote Sensing, 8(4), p.333.

812 *Table 1. Data products and sources (National Ecological Observatory Network, 2016).*

813 *Information about data products can be found on the NEON data products catalogue*

814 *(http://data.neonscience.org/data-product-catalog).*

Name	NEON data product ID	Data date	How it was used
Spectrometer orthorectified at-sensor radiance	NEON.DP1.30008	2014 and 2015	Hyperspectral images used to model foliar chemical and physical properties
Discrete return LiDAR point cloud	NEON.DP1.30003.001	2014 and 2015	Crown segmentation and calculation of tree height
AOP L2 and L3 data products (Albedo, Elevation, Slope, Aspect)	NEON.DP2.30012.001, DP3.30024.001, DP3.30025.001	2014 and 2015	Link modeled tree crown properties with other NEON-AOP data products
Woody plant vegetation structure	DP1.10098.001	2014-2018	Build allometric relationship to infer DBH from Crown Area and Tree Height
Field ITC	Graves et al. 2018	2017	Validate crown segmentation, define tree objects.

815

Figures captions

Figure 1. *Workflow of the pipeline following Unified Modeling Language (UML). Left side shows the method to build and test three modeling approaches: PBM (pixel-based model), EPBS (ensemble of pixel-based models), CEAM (crown ensemble averaged model). Right side represents the part of the pipeline dealing with scaling, fusion, and public distribution of derived data. NEON L3 products fused to the derived traits data are: Aspect (DP3.30025.001), Elevation (DP3.30024.001), and Slope (DP3.30025.001).*

Figure 2. *Comparison between observed and predicted tree structural traits for algorithmically delineated crowns corresponding to ground delineated ITCs: (A) tree crown height (m), (B) tree diameter at breast height (cm), and (C) tree crown area (m2). Yellow and blue points represent OSBS and TALL site data points respectively. Black diagonal is the 1:1 line.*

Figure 3. *Model evaluation and comparison of pixel based (SPM, red), ensemble pixels (EPBM, grey), crown spectra average (CAS, yellow), and crown ensemble average (CEAM, blue) predictions on an independent test set of 24 observed crowns for %P, LMA, %N and %C. (A) Evaluation and comparison of RMSE from models built on pixels extracted from ground delineated crowns; (B) Evaluation and comparison of RMSE from models built on pixels extracted from algorithmically delineated crowns; (C) difference in performance (RMSE) between models tested on pixels extracted from field and algorithmically delineated crowns. Positive values mean that for that comparison model built on automatically delineated crowns performed better. (D) Coverage of the 95 predictions intervals on held out data for the four*

838 *models (LMA, N, P and C). Dash-dotted line represent the ideal coverage value of 95%.*

839 ***Figure 4.*** *Example of predictions at the landscape scale for individual tree crowns (ITC) at*
840 *Ordway Swisher Biological Station (OSBS). In the center, predictions of tree height for ~2.5*
841 *million trees within NEON AOP footprint (215 km2), plotted in a quantile scale using the viridis*
842 *color palette. Cropped images represent a ~1 km2 detail of LMA, %N, %C, and %P predictions*
843 *at scale. Expected values are presented on a quantile scale using a spectral color palette (with*
844 *lower values in red, and higher values in blue). Range of the 95% probability intervals for the*
845 *same area are presented on the intensity scale of blues (with lower values in white, and higher*
846 *values in deep blue).*

847
848 ***Figure 5.*** *Leaf chemical distributions and relationship with tree height on a random sample of*
849 *100,000 derived individual tree crowns (ITCs). On the top row, comparison between*
850 *distributions of C, LMA, %P, and %N for the two sites, OSBS (blue), and TALL (yellow).*
851 *Vertical dotted lines represent the average for the site. Rug plots on the x-axis represent the*
852 *marginal distribution of OSBS and TALL data between the minimum and maximum range of*
853 *derived observations. On the lower row, example of relationship between tree height and the*
854 *same three leaf chemical traits: from left to right, LMA, %N, %P. Linear trends and 95CI*
855 *ellipses are represented for each relationship and site, following the same color scheme as*
856 *above.*

857

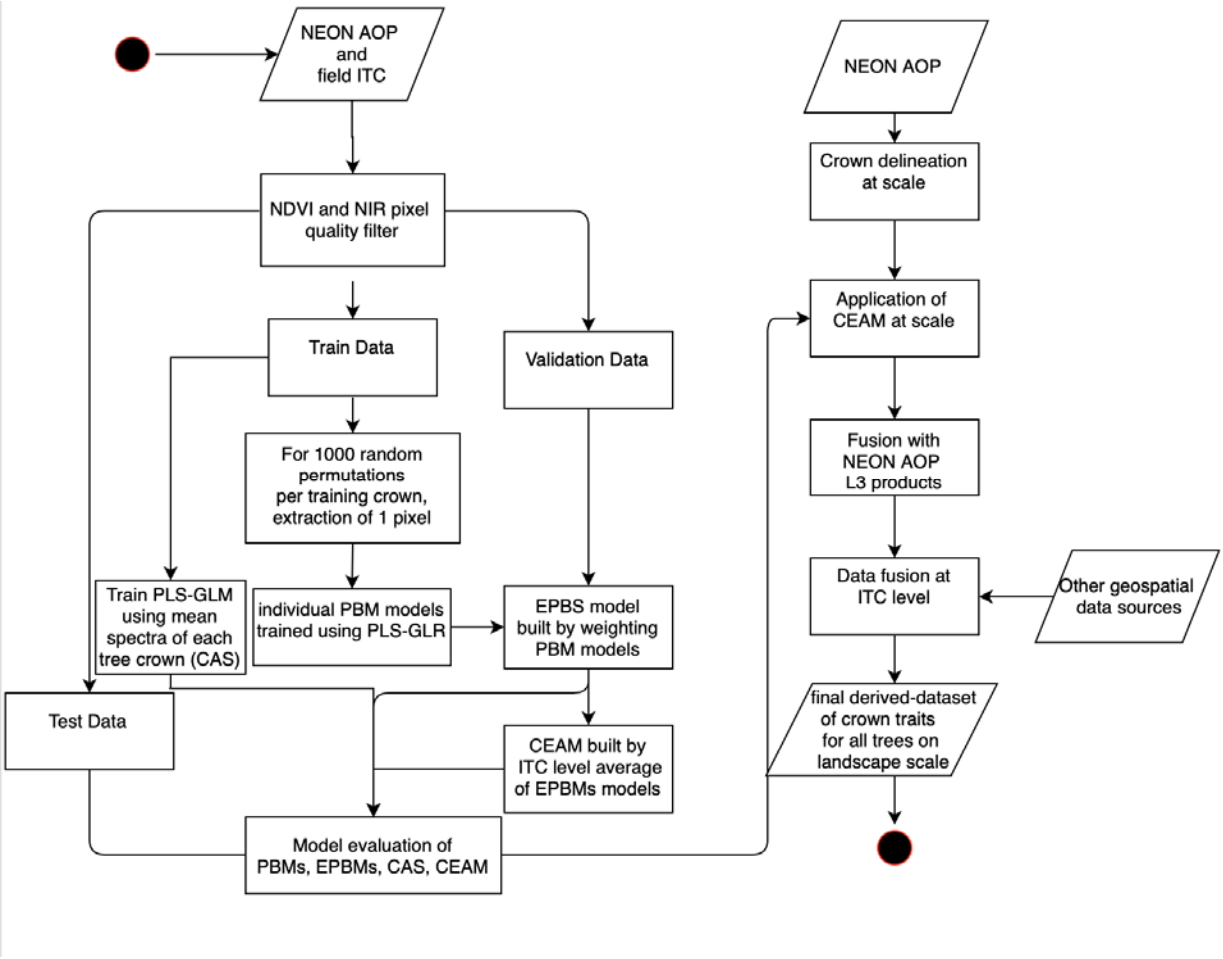

Figure 1. Workflow of the pipeline following Unified Modeling Language (UML). Left side shows the method to build and test three modeling approaches: PBM (pixel-based model), EPBS (ensemble of pixel-based models), CEAM (crown ensemble averaged model). Right side represents the part of the pipeline dealing with scaling, fusion, and public distribution of derived data. NEON L3 products fused to the derived traits data are: Aspect (DP3.30025.001), Elevation (DP3.30024.001), and Slope (DP3.30025.001).

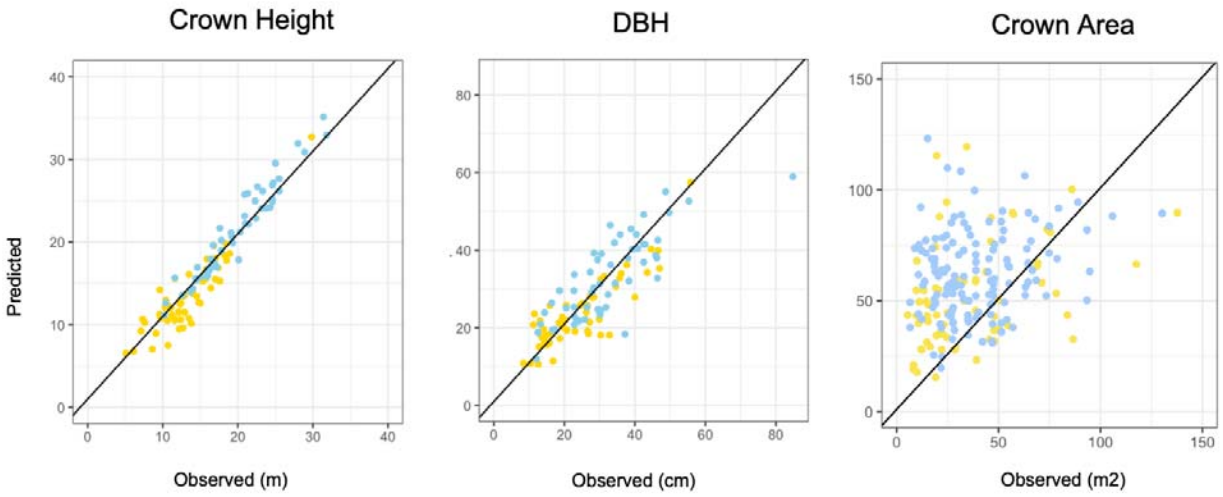

869

870 *Figure 2. Comparison between observed and predicted tree structural traits for algorithmically*

871 *delineated crowns corresponding to ground delineated ITCs: (A) tree crown height (m), (B) tree*

872 *diameter at breast height (cm), and (C) tree crown area (m2). Yellow and blue points represent*

873 *OSBS and TALL site data points respectively. Black diagonal is the 1:1 line.*

874
875

876

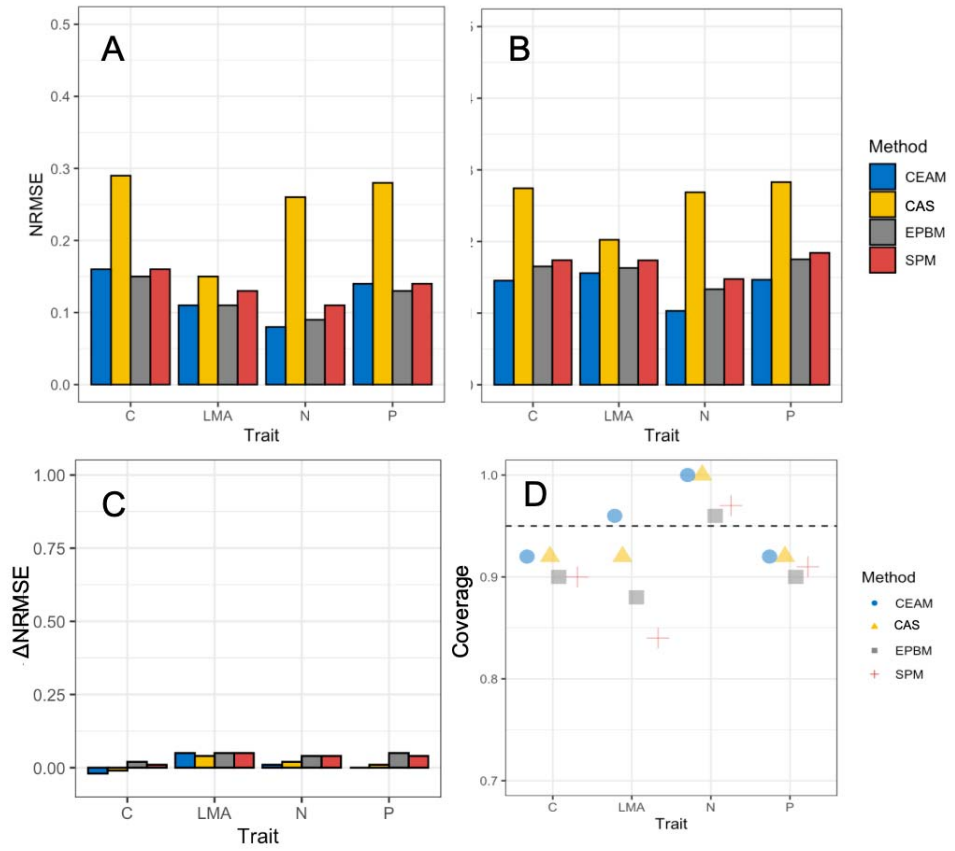

877
878 *Figure 3. Model evaluation and comparison of pixel based (SPM, red), ensemble pixels (EPBM,*
879 *grey), crown spectra average (CAS, yellow), and crown ensemble average (CEAM, blue)*
880 *predictions on an independent test set of 24 observed crowns for %P, LMA, %N and %C. (A)*
881 *Evaluation and comparison of RMSE from models built on pixels extracted from ground*
882 *delineated crowns; (B) Evaluation and comparison of RMSE from models built on pixels*
883 *extracted from algorithmically delineated crowns; (C) difference in performance (RMSE)*
884 *between models tested on pixels extracted from field and algorithmically delineated crowns.*
885 *Positive values mean that for that comparison model built on automatically delineated crowns*
886 *performed better. (D) Coverage of the 95 predictions intervals on held out data for the four*
887 *models (LMA, N, P and C). Dash-dotted line represent the ideal coverage value of 95%.*

888

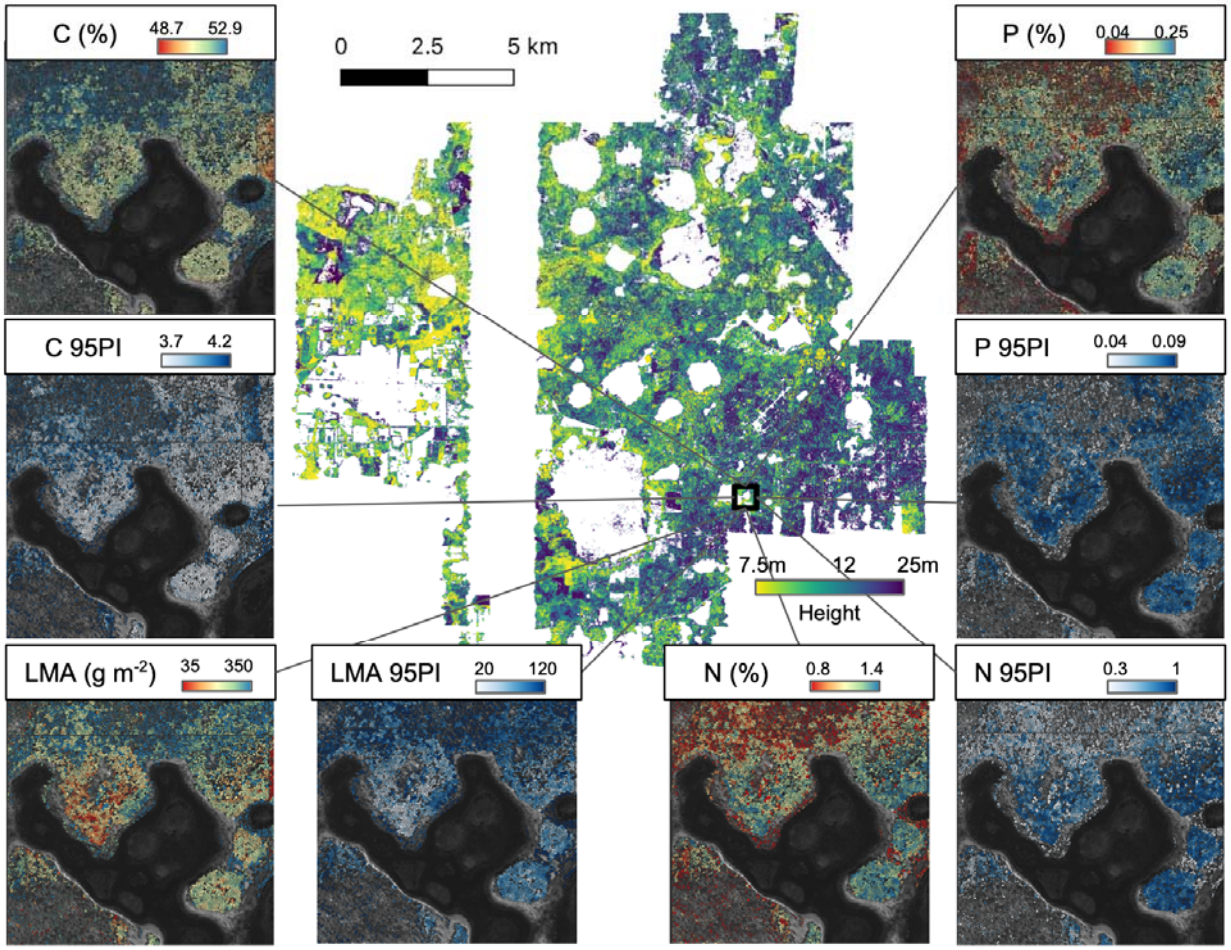

Figure 4. Example of predictions at the landscape scale for individual tree crowns (ITC) at Ordway Swisher Biological Station (OSBS). In the center, predictions of tree height for ~2.5 million trees within NEON AOP footprint (215 km2), plotted in a quantile scale using the viridis color palette. Cropped images represent a ~1 km2 detail of LMA, %N, %C, and %P predictions at scale. Expected values are presented on a quantile scale using a spectral color palette (with lower values in red, and higher values in blue). Range of the 95% probability intervals for the same area are presented on the intensity scale of blues (with lower values in white, and higher values in deep blue).

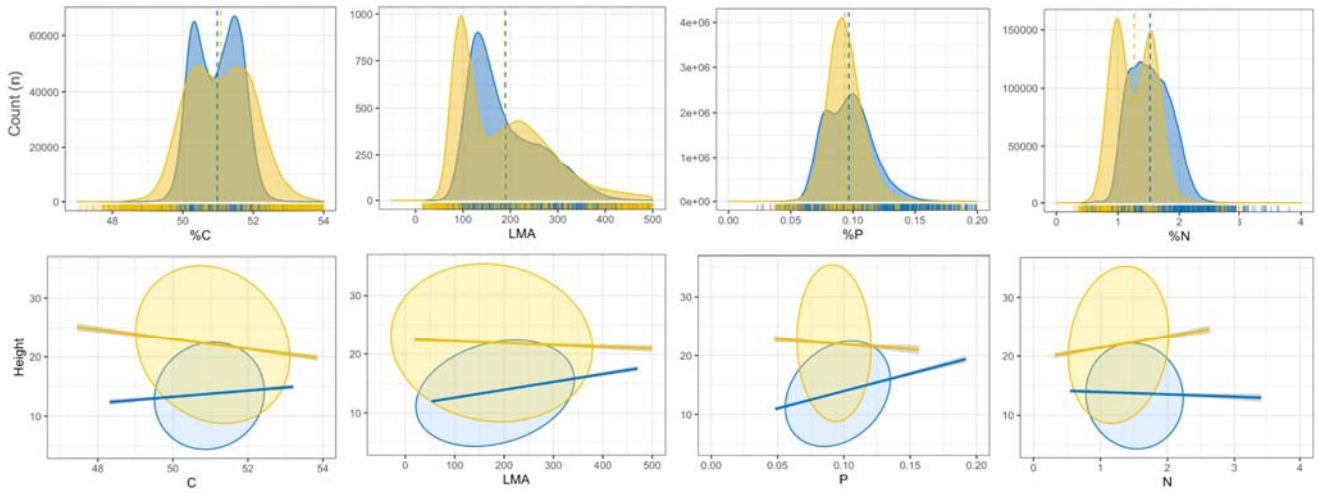

Figure 5. Leaf chemical distributions and relationship with tree height on a random sample of 100,000 derived individual tree crowns (ITCs). On the top row, comparison between distributions of C, LMA, %P, and %N for the two sites, OSBS (blue), and TALL (yellow). Vertical dotted lines represent the average for the site. Rug plots on the x-axis represent the marginal distribution of OSBS and TALL data between the minimum and maximum range of derived observations. On the lower row, example of relationship between tree height and the same three leaf chemical traits: from left to right, LMA, %N, %P. Linear trends and 95CI ellipses are represented for each relationship and site, following the same color scheme as above.